

Abnormal Static and Dynamic Local Functional Connectivity in First-Episode Schizophrenia: A Resting-State fMRI Study

Jie Zhou, Xiong Jiao¹, Qiang Hu, Lizhao Du¹, Jijun Wang, and Junfeng Sun¹, *Senior Member, IEEE*

Abstract—Dynamic functional connectivity (FC) analyses have provided ample information on the disturbances of global functional brain organization in patients with schizophrenia. However, our understanding about the dynamics of local FC in never-treated first episode schizophrenia (FES) patients is still rudimentary. Dynamic Regional Phase Synchrony (DRePS), a newly developed dynamic local FC analysis method that could quantify the instantaneous phase synchronization in local spatial scale, overcomes the limitations of commonly used sliding-window methods. The current study performed a comprehensive examination on both the static and dynamic local FC alterations in FES patients (N = 74) from healthy controls (HCs, N = 41) with resting-state functional magnetic resonance imaging using DRePS, and compared the static local FC metrics derived from DRePS with those calculated from two commonly used regional homogeneity (ReHo) analysis methods that are defined based on Kendall's coefficient of concordance (KCC-ReHo) and frequency coherence (Cohe-ReHo). Symptom severities of FES patients were assessed with a set of clinical scales. Cognitive functions of FES patients and HCs were assessed with the MATRICS consensus cognitive battery. Group-level analysis revealed that compared with HCs, FES patients exhibited increased static local FC in right superior, middle temporal gyri, hippocampus, parahippocampal gyrus, putamen, and bilateral caudate nucleus. Nonetheless, the dynamic local FC metrics did not show

any significant differences between the two groups. The associations between all local FC metrics and clinical characteristics manifested scores were explored using a relevance vector machine. Results showed that the Global Assessment of Functioning score highest in past year and the Brief Visuospatial Memory Test-Revised task score were statistically significantly predicted by a combination of all static and dynamic features. The diagnostic abilities of different local FC metrics and their combinations were compared by the classification performance of linear support vector machine classifiers. Results showed that the inclusion of zero crossing ratio of DRePS, one of the dynamic local FC metrics, alongside static local FC metrics improved the classification accuracy compared to using static metrics alone. These results enrich our understanding of the neurocognitive mechanisms underlying schizophrenia, and demonstrate the potential of developing diagnostic biomarker for schizophrenia based on DRePS.

Index Terms—Dynamic regional phase synchrony, regional homogeneity, coherence, local functional connectivity, resting-state fMRI.

I. INTRODUCTION

SCHIZOPHRENIA is a complicated mental disorder with multiple symptoms and numerous interacting risk factors [1]. The heterogeneous genetic, neurobiological, and phenotypical profiles among schizophrenia patients challenge the current diagnostic criteria, which are primarily defined based on clinical phenomenology and illness course [2]. Thus, it is important to identify objective and schizophrenia-specific biological biomarkers. Neuroimaging provides a promising avenue for exploring such biomarkers [3]. Although structural and functional brain alterations in schizophrenia revealed by neuroimaging techniques have provided valuable insights about this disease, the interpretation and translation of these heterogeneous findings into clinical applications are still challenging [4], [5]. Machine learning analysis has the advantages of characterizing brain abnormalities at the individual level and evaluating multiple variables simultaneously, which makes it valuable for examining the diagnostic value of neuroimaging findings and establishing associations between the behavioral or cognitive features of patients and multiple brain abnormalities [6], [7], [8], [9], [10].

Resting-state functional magnetic resonance imaging (rs-fMRI) is a noninvasive, task-free neuroimaging technology

Manuscript received 24 August 2023; revised 15 December 2023 and 3 February 2024; accepted 16 February 2024. Date of publication 22 February 2024; date of current version 1 March 2024. This work was supported in part by the National Natural Science Foundation of China under Grant 61976136, Grant U20B2074, and Grant 62376157; and in part by the Specific Project of Shanghai Jiao Tong University for "Invigorating Inner Mongolia through Science and Technology" under Grant 2022XYJG0001-01-21. (Corresponding authors: Junfeng Sun; Jijun Wang.)

This work involved human subjects or animals in its research. Approval of all ethical and experimental procedures and protocols was granted by the Ethics Committee of Shanghai Mental Health Center under Application No. 2017-24R1 and the Ethics Committee of First Psychiatric Hospital of Harbin under Application No. IRB2019-004.

Jie Zhou, Xiong Jiao, Lizhao Du, and Junfeng Sun are with the School of Biomedical Engineering, Shanghai Jiao Tong University, Shanghai 200240, China (e-mail: jfsun@sjtu.edu.cn).

Qiang Hu is with the Department of Psychiatry, Zhenjiang Mental Health Center, Zhenjiang, Jiangsu 212003, China.

Jijun Wang is with Shanghai Key Laboratory of Psychotic Disorders, Shanghai Mental Health Center, Shanghai Jiao Tong University School of Medicine, Shanghai 200030, China (e-mail: jijunwang27@163.com).

This article has supplementary downloadable material available at <https://doi.org/10.1109/TNSRE.2024.3368697>, provided by the authors. Digital Object Identifier 10.1109/TNSRE.2024.3368697

that is believed to reflect the intrinsic neural activity. The seminal study concluded that the correlation of low-frequency blood oxygenation level dependent (BOLD) signal in the resting-state brain manifests functional connectivity (FC) of the brain [11]. A variety of FC analysis approaches and measures have been developed and deployed in schizophrenia research, such as regional homogeneity (ReHo) [12], [13], [14], [15], amplitude of low-frequency fluctuations (ALFF) [16], [17], graph theory-based connectivity analysis [18], and dynamic FC analysis [19], [20], [21], [22], [23], [24]. The dynamic FC analysis aims to characterize time-varying features of FC. Nowadays, most of dynamic FC analysis conducted in schizophrenia research aims to reveal the fluctuation laws of network-level attributions, such as brain state repertoires based on correlation patterns between remote brain regions [22] and topological properties of brain network [25], [26]. While, the local FC fluctuations in rs-fMRI research was largely unexplored [27], [28]. Some relevant clinical studies captured the fluctuations of ReHo or ALFF across sliding windows to detect the altered dynamic intrinsic brain activity in Alzheimer [29], major depressive disorder [30], stroke [31] and schizophrenia [32] patients. Results in these studies validated the potential of dynamic local FC in revealing the underlying mechanism of brain diseases. However, such study is still in its infancy, and also suffered from limitations and uncertainties existed in the analysis based on sliding window [33], [34].

Aberrant neural dynamics can be considered as primary and fundamental pathophysiology in schizophrenia [35]. For examples, electrophysiological studies based on EEG signals have reported the dynamics of highly reproducible [36] and the abnormal amplitude dynamics of EEG oscillations [37] in schizophrenia patients. Compared with EEG, fMRI has higher spatial resolution but lower temporal resolution. For study based on fMRI, dynamic local FC analysis with improved temporal resolution may reveal new information of aberrant neural dynamics in schizophrenia. Dynamic Regional Phase Synchrony (DRePS), a local FC analysis approach developed in recent years, utilizes instantaneous local mean phase coherence within adjacent fMRI voxels to measure the instantaneous fluctuation of local FC [38]. This instantaneous measure has high temporal resolution (i.e., up to the sampling interval $TR = 2$ s in this study) and thus overcomes the constraints of the analysis based on sliding window. DRePS has been successfully applied in clinical research on generalized anxiety disorder [39], neocortical focal epilepsy [40], and depression disorder [41]. However, DRePS has rarely been applied in schizophrenia research yet.

The characteristics of local FC fluctuations depicted by DRePS time series can provide both dynamic and static information of local FC. The dynamic properties of DRePS time series have been characterized with its average spectral density [40] and its standard deviation [39] in previous studies. While more dynamic information contained in DRePS time series remains to be explored. In this study, we introduce a new metric named the zero crossing ratio of DRePS, inspired from the concept of zero crossing in signal processing [42]. This metric quantifies the frequency at which a DRePS time series

deviates from its mean level. The static information of DRePS time series is mainly included in its temporal average (mean-DRePS) [38], which has been shown to have high positive linear correlation with ReHo [28], [40].

ReHo is a widely accepted measure for assessing the local FC alteration in schizophrenia. There are two commonly used definitions, one is the original definition of ReHo (KCC-ReHo) that is defined by the Kendall's coefficient of concordance based on amplitude rank [43], [44], the other is the Cohe-ReHo that is defined by the frequency coherence [45]. Compared with these two ReHo definitions, DRePS is based on the local synchronization of the instantaneous phase of voxels in neighborhood. These three measures are defined from three different perspectives, i.e., rank of amplitude, frequency coherence, and instantaneous phase synchronization, respectively, and thus could be expect to provide complementary information to each other. This commonality allows for the comparison and integration of all metrics calculated from them at a regional spatial level. By simultaneously examining a brain region using these comprehensive pieces of information, we could anticipate to enhance our understanding of regional functional alterations in FES patients. With this consideration, we would also perform local FC analysis with KCC-ReHo and Cohe-ReHo, and compare the results by KCC-ReHo and Cohe-ReHo with those by DRePS, thus providing a comprehensive understanding of the static and dynamic alterations of local FC in FES patients from the perspectives of amplitude rank, frequency coherence, and instantaneous phase synchronization.

In this study, we examined the alterations of local FCs in FES patients by using the dynamic local FC metrics including the average of power spectral density of DRePS (psd-DRePS), the variance of DRePS (var-DRePS) and the zero crossing ratio of DRePS (zcr-DRePS), and the static local FC metrics including mean-DRePS, KCC-ReHo, and Cohe-ReHo. We also investigated the association of all these metrics with symptom/cognitive scores respectively, using a multivariate sparse relevance vector machine (RVM) model. Furthermore, we explored the diagnostic value of different combination of metrics of local FC with a linear support vector machine (SVM) model. We expected that the dynamic metrics of local FC could offer valuable insights into the underlying mechanisms of schizophrenia beyond the static metrics of local FC.

II. MATERIALS AND METHODS

A. Demographic and Clinical Characteristics

Totally, this study included 74 FES patients and 41 HCs (Table 1). All subjects were recruited from Psychiatric Department of the First Psychiatric Hospital of Harbin. The study was approved by the Ethics Committee of Shanghai Mental Health Center (No. 2017-36R; date: 13th, Aug., 2018) and the First Psychiatric Hospital of Harbin, and has been registered with the Chinese Clinical Trial Register Center (Registration number: ChiCTR2000041106). FES patients met the following inclusion criteria: (i) diagnosed by an experienced psychiatrist according to the criteria for schizophrenia in Diagnostic and Statistical Manual of Mental Disorders,

TABLE I
THE DEMOGRAPHIC INFORMATION, NEUROCOGNITIVE PERFORMANCES AND SYMPTOMS OF PARTICIPANTS INCLUDED IN ANALYSES

Characteristics	FES (N=74)	HCS (N=41)	t or χ^2 statistics	P value
Age, years	27.22±7.93	27.16±8.15	0.330	0.974
Gender, male/female	38/36	20/21	0.070	0.790
Education, years	11.26±3.99	12.90±2.66	-2.350	*
Head motion	0.073±0.03	0.068±0.033	0.680	0.490
Neurocognitive performances				
TMT	43.14±13.14 (N=71)	54.98±6.51 (N=40)	-6.330	***
BACS-SC	44.56±7.86 (N=71)	55.98±6.43 (N=40)	-7.820	***
HVLT-R	45.46±11.08 (N=71)	53.10±7.29 (N=40)	-3.904	***
BVMT-R	46.41±10.72 (N=71)	55.18 ±8.80 (N=40)	-4.586	***
WMS-III: SS	44.38±12.19 (N=71)	50.38 ±8.39 (N=40)	-3.053	**
Maze	46.21±11.51 (N=71)	55.53±7.54 (N=40)	-4.402	***
CPT-IP	43.66±8.95 (N=68)	53.54±6.17 (N=39)	-4.586	***
Fluency	50.08±10.22 (N=71)	54.90±9.16 (N=40)	-2.472	**
MSCEIT ME	33.79 ±5.52 (N=61)	36.85±5.78 (N=40)	-2.677	***
FES Symptoms				
HAMA total	12.16±3.52 (N=74)	PANSS total	81.47±11.83 (N=74)	
HAMD total	18.59±5.03 (N=74)	PANSS Positive	20.14 ±4.00 (N=74)	
GAF score of current situation	34.96±7.10/ (N=74)	PANSS Negative	22.27±5.94 (N=74)	
GAF highest in past year	66.07±12.61 (N=74)	PANSS General	39.38±6.33 (N=74)	
CGI score	4.59±0.68 (N=74)			

Note: values are presented as mean ± SD. N represents the total number of participants who completed specific neurocognitive test or symptom assessments. Group differences were mainly compared using two-sample t-tests, and group difference in sex was compared using Chi-square tests. The significant level was set as * p<0.05, ** p <0.01, *** p<0.001.

Fifth Edition (DSM-V) [46]; (ii) age of 15-45 years and IQ>69; (iii) overall clinical global impression (CGI) scale≥4; (iv) the total score of positive and negative syndrome scale (PANSS) ≥60; (v) first onset without previous systemic anti-psychotic treatment. Written informed consent of the FES patient was obtained from his/her legally authorized representative, and HCs provided written informed consent himself/herself, after totally understanding the purpose of our study.

The positive and negative syndrome scale (PANSS) was used to assess the symptom severity of FES patients. The Hamilton depression scale (HAMD-24) and Hamilton anxiety scale (HAMA-14) were used to assess the depression and anxiety symptoms of FES patients respectively. Clinical global impression (CGI), global assessment of functioning (GAF) scores for the current situation, and GAF for highest level in past years were used to assess the severity of the disease and the overall function of FES patients. MATRICS Consensus Cognitive Battery (MCCB) was implemented to assess the cognition of all participants on the basis of nine

neurocognitive sub-tests, including the Trail Making Test (TMT), Brief Assessment of Cognition in Schizophrenia Symbol Coding Test (BACS-SC), Hopkins Verbal Learning Test-Revised (HVLT-R), Wechsler Memory Scale-III: Spatial Span (WMS-III: SS), Neuropsychological Assessment Battery (Maze), Brief Visuospatial Memory Test-Revised (BVMT-R), Category Fluency Test (Fluency), Continuous Performance (CPT-IP) and Mayer-Salovey-Caruso Emotional Intelligence Test: Managing Emotions (MSCEIT ME).

B. Image Acquisition and Processing

Structural MRI and fMRI data of all subjects were collected in a 3.0T MRI scanner (GE Discovery MR750) with a 32-channel radio frequency coil. All subjects were instructed to remain relaxed, stationary, motionless and awaked with eye open. To reduce head motion artifacts, sponges were used to fix subject's head during scanning process. T1 weighted structural images were acquired with a 3D turbo spin echo sequence in axial orientation with repetition time (TR) = 8.208s, echo time (TE) = 2.32s, flip angle = 12, slice thickness = 1mm, matrix = 512 × 512, and slice number = 184. The fMRI images were collected using an echo-planar imaging sequence with the following parameters: TR = 2 s, TE = 45ms, sagittal slice number = 32, matrix = 64 × 64, flip angle = 90, field of view = 220mm, slice thickness = 4mm, and voxel size = 3.125mm × 3.125 mm × 4.5mm. The fMRI scan lasted for 6 min and 180 volumes was acquired in total.

The fMRI data were preprocessed using the DPABI toolbox (DPABI V6, <http://rfmri.org/dpabi>) [47] and statistical parametric mapping 12 (SPM12) [48]. The first five volumes were discarded to prevent the effect of initial fMRI signal instability and participant maladaptation. The remaining 175 volumes were processed through the following steps: slice time correction based on the acquisition time delay between slices; head motion correction by realigning all volumes to the mean image; space registration according to the transform parameters calculated by registering fMRI image and T1 image; segmentation of different brain tissues via DARTEL algorithm; regressing out nuisance covariates (i.e., linear trend, Friston 24 head motion parameters, white matter signal, cerebrospinal fluid signal); normalizing to the MNI space using an echo-planar imaging (EPI) template; resampling processed image to 3mm isotropic voxels, and band-pass filtering (0.01-0.08HZ). Spatial smoothing was not performed in the preprocessing stage. For quality control, the subjects who meets any of the following conditions were excluded: (i) raw images have obvious scanner artifacts; (ii) raw images do not cover the whole brain; (iii) spatial normalization failed; and (iv) excessive head motion (mean frame wise displacement larger than 0.2 mm, Jenkinson version). In total, nine FES patients and five HCs were excluded from the original sample size of 83 FES patients and 46 HCs, resulting in a final sample size of 74 FES patients and 41 HCs. An intersection gray mask which included 90 percent of total participants was made, and only the voxels within this mask were taken for further standardization process and statistical analysis.

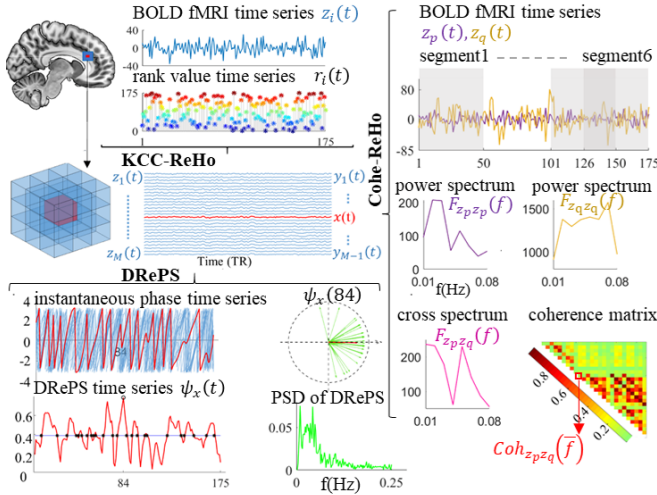


Fig. 1. Illustrations of the calculation process of KCC-ReHo, Cohe-ReHo and DRePS time series.

C. Calculation of Local FC Metrics

For a given voxel, its spatially adjacent neighborhood could be defined with a 3-dimensional (3D) cubic box ($3 \times 3 \times 3$), and its local synchronization was measured with KCC-ReHo, Cohe-ReHo, and DRePS respectively (Fig. 1). In the calculation of KCC-ReHo and Cohe-ReHo, we used $z_i(t)$, $i = 1, 2, \dots, M, t = 1, 2, \dots, N$, to represent the fMRI time series of all voxels in the cubic box, where M denotes the number of voxels and N denotes the length of fMRI time series. In the calculation of DRePS, we used $x(t)$ to represent the fMRI time series of the central voxel of the cubic box and $y_j(t)$, $j = 1, 2, \dots, M-1, t = 1, 2, \dots, N$ to represent fMRI time series of the neighboring voxels of $x(t)$. Our homemade codes for local FC metrics calculation were mainly adapted from the RESTplus toolkit [49] and the codes provided by the author who proposed the DRePS method [38].

KCC-ReHo was calculated by the rank-based Kendall's coefficient of concordance [43]. For each $z_i(t)$, all the values in fMRI time series were sorted by amplitude and its corresponding rank series $r_i(t)$ was obtained, where $r_i(t)$ denotes the rank value of the i -th voxel at the t -th time point. The KCC value was calculated by Eq. (1),

$$\text{KCC} = \frac{\sum_{t=1}^N [R(t)]^2 - N(\bar{R})^2}{M^2(N^3 - N)}, \quad (1)$$

where $R(t) = \sum_{i=1}^M r_i(t)$, and $\bar{R} = \frac{1}{N} \sum_{t=1}^N R(t)$. Then it was assigned to the given voxel as the KCC-ReHo metric.

To calculate Cohe-ReHo [45], the power spectrum $F_{z_i}(f)$ of each $z_i(t)$ and the cross spectrum $F_{z_p z_q}(f)$ of all voxel pairs, i.e., $z_p(t)$, $z_q(t)$, $p, q \in i$ and $p \neq q$ in the neighborhood, were estimated using Welch's modified periodogram averaging method. The detailed calculation process was as follows: each time series were divided into six segments (50 time points each segment) with 50% overlapping; each segment was then mean-centered and weighted by Hanning window; the discrete Fourier transform (DFT) of the k -th segment of time series $z_i(t)$ was calculated and represented as $Z_{ik}(f)$,

$f = 0.01, 0.02, \dots, 0.25$ Hz, $k = 1, 2, \dots, 6$; based on the DFT $Z_{ik}(f)$ of voxel z_i , the power spectrum of each low frequency components ($f = 0.01, 0.02, \dots, 0.08$ Hz) was estimated as the average of the power spectra of the $K = 6$ segments, i.e.,

$$F_{z_i z_i}(f) = \frac{1}{K} \sum_{k=1}^K Z_{ik}(f) \cdot Z_{ik}^{*(T)}(-f), \quad (2)$$

where $Z_{ik}^{*(T)}(-f)$ represents the complex conjugate transpose of $Z_{ik}(f)$. Based on the DFT $Z_{pk}(f)$ and $Z_{qk}(f)$ of paired voxels z_p and z_q , we can estimate their cross spectrum of each low-frequency components as

$$F_{z_p z_q}(f) = \frac{1}{K} \sum_{k=1}^K |Z_{pk}(f) \cdot Z_{qk}^{*(T)}(-f)|. \quad (3)$$

Then the coherence of any voxel pair z_p and z_q across the low-frequency band (0.01-0.08 Hz) can be estimated as follows:

$$\text{Coh}_{z_p z_q}(\bar{f}) = \frac{\left| \sum_f F_{z_p z_q}(f) \right|^2}{\sum_f F_{z_p z_p}(f) * \sum_f F_{z_q z_q}(f)}. \quad (4)$$

With the estimated coherence of all voxels pairs, the mean of all the estimated coherence was calculated as Cohe-ReHo metric and assigned to the given voxel.

To calculate DRePS time series [28], [38], the instantaneous phases of central voxel x and its neighboring voxels (y_j , $j = 1, 2, \dots, M-1$), denoted by $\varphi_x(t)$ and $\varphi_{y_j}(t)$ respectively, were first extracted from the detrended and filtered fMRI time series using the Hilbert transform [50]. Then the DRePS value at time t of the central voxel x was calculated as the instantaneous mean phase coherence according to Eq. (5), as shown at the bottom of the next page.

For each voxel, the DRePS time series was calculated according to Eq. (5). Both static and dynamic characteristics of each DRePS time series were quantified using various statistical descriptions. The mean value of the DRePS time series was used as a static metric, while the fluctuations of the DRePS time series were quantified using the variance (var-DRePS), the average power spectral density (psd-DRePS), and the zero-crossing ratio relative to its mean value (zcr-DRePS). In detail, for var-DRePS, the variance of the DRePS time series was normalized by $(N - 1)$, which aligns with the default setting of the *var* function in the Matlab toolbox. The calculation of psd-DRePS followed the steps outlined in [40]: the mean of the DRePS time series was first detrended; then the Fast Fourier Transform (FFT) of the time detrended DRePS series was computed; the power spectrum was further obtained by squaring the absolute value of the FFT, and the psd-DRePS value was reached by averaging the power spectrum across the entire frequency spectrum. The calculation of zcr-DRePS was based on the method in [42], which involves the following steps: detrending the mean of the DRePS time series; identifying the total number of zero-crossing points, which change their sign from positive to negative or vice versa in the detrended DRePS time series; and finally getting the zcr-DRePS value by dividing the total number of the zero-crossing points by the total length of the fMRI data.

D. Statistical Analysis

1) *Group Difference Analysis*: Before statistical analysis, all the local FC metrics were transformed into standard Z value (subtracting the global mean, then being divided by global standard deviation) to improve their normality of distribution [45], [51]. The global mean and standard deviation for a specific local FC metric of any participant were calculated from the mean and standard deviation of the corresponding values of all voxels under the 90 percent group gray mask [47]. Then, the standardized whole brain local FC metric maps were smoothed using a Gaussian kernel with a full width at half-maximum of 8mm. To detect group differences between FES patients and HCs for each local FC metric, we applied a two-sample t-test analysis on corresponding standardized and smoothed brain maps while controlling age, gender, years of education (EDU), and head motion (mean Jenkinson frame displacement) as covariates. This voxel-wise statistical analysis was performed using the DPABI toolbox [47]. Statistical results were corrected for multiple comparison using false discovery rate (FDR). Voxel clusters with more than 10 voxels surviving the multiple comparison correction were identified and selected as regions of interest (ROIs), which were named by the Automated Anatomical Labeling (AAL) atlas [52] where its peak voxel locates. The value of each ROI was calculated by taking the average of the raw value of related metric across all voxels within it.

2) *Univariate Correlation Analysis*: The partial correlations of the identified abnormal ROIs with respect to the symptom severities of FES patients were analyzed using age, gender, EDU and mean frame displacement (FD) as covariates. The partial correlations between ROIs and cognitive scores of all participants were further quantified, using age, gender, EDU, mean FD and group information as covariates. The multiple comparisons were corrected by the Bonferroni correction. That is, the statistical level at $p < 0.05/L$ was considered significant, where L is the number of ROIs.

3) *Feature Preparation for Machine Learning Analysis*: Brain was parcellated into 90 regions according to the AAL atlas [52]. For each local FC metric, the average of its raw values across voxels within each atlas-defined brain regions was calculated as a feature. The so calculated features were further used in prediction and classification analyses.

4) *Prediction Analysis With Relevance Vector Machine*: The purpose of the prediction analysis was to investigate the relationships between cognitive/symptom scores and the features of all metrics simultaneously. We employed the RVM model [53] with a 100 repeated 5-fold cross-validation strategy, and evaluated its performance using Pearson's correlation between the covariate-adjusted scores and their predicted values. The significance of the RVM's performance was evaluated using a permutation test by shuffling target scores

1000 times. The model fitting and evaluation mainly referred to [10], which employed a k-fold cross-validation procedure and implemented confounding regression on both the dependent and independent variables.

- S1) For each prediction process, the prepared features of all metrics were used as independent variables, while a symptom or cognitive score was used as dependent variable. In the symptom prediction, the confounding variables were age, gender, education year, and head motion (mean Jenkinson FD). In the cognitive prediction, the group information was also included as confounding variable.
- S2) In each repeated process, a 5-fold cross-validation was implemented. The dataset formed by independent variables and dependent variable was divided into 5 folds, and each fold served as the testing set once, while the remaining folds served as the training set. Thus, a cross-validation process included five loops.
- S3) In each cross-validation loop, before applying the RVM model, a preprocessing step was included to adjust the effect of aforementioned confounding variables. The regression coefficients were learned on the training set with a confound regression model and then applied to training set and testing set simultaneously. This arrangement was made to avoid data leakage problem. Then, the RVM model was trained on confound-adjusted training set and tested on confound-adjusted independent variables in testing set to predict the dependent variable.
- S4) The prediction performance of each cross-validation loop was evaluated by the Pearson's correlation calculated between the predicted dependent variables and cofound-adjusted dependent variables in testing set. The prediction performance of one repeated process of 5-fold cross-validation was evaluated by the average of the Pearson's correlation coefficients calculated across the 5 loops in the cross-validation process. The prediction performance of the whole prediction process was evaluated by the average of the performance of the 100 repeated cross-validations.
- S5) Permutation test (1000 times) was used to determine if the prediction of the corresponding score was higher than by chance. We randomly shuffled the dependent variable in step S1, and repeated steps S2-S4 for 1000 times. Among these 1000 repetitions, if there are no more than 50 times that the prediction performance of the permuted data exceeded the result of true data, then the significant level was achieved (i.e., $p < 0.05$).

The RVM model is derived from a specialized version of a general Bayesian framework. One of its most important characteristics is its ability to produce sparse learned predictors, that is, only a few input features are assigned non-zero weights

$$\psi_x(t) = \frac{1}{M-1} \sqrt{\left\{ \sum_{j=1}^{M-1} \cos(\varphi_x(t) - \varphi_{y_j}(t)) \right\}^2 + \left\{ \sum_{j=1}^{M-1} \sin(\varphi_x(t) - \varphi_{y_j}(t)) \right\}^2}. \quad (5)$$

in the RVM model. This sparsity property helps identify the most contributive features in prediction. To quantify the contribution of each feature to the prediction, we calculated the ratio of features assigned non-zero weights across the 100×5 training processes.

5) *Classification Analysis With Support Vector Machine*: The purpose of classification analysis is to examine whether the dynamic metrics helps in classification between FES patients and HCs. For this purpose, we applied SVM on features of single type metric, features of paired metrics, and features of different combinations of metrics. The design of classification process mainly referred to reference [22]. Classifiers were applied to various dataset formed with different feature sets (Table III). For each dataset, the number of input features was represented by J , the number of sample was represented by S . The whole analysis process mainly included three parts: determining the best feature selection number Q , computing the classification performance of the given dataset with the Q parameter, and performing the permutation test with the Q parameter. All the three parts relayed on the same leave-one-out cross-validation (LOOCV) procedure.

- S1) The LOOCV procedure embedded a ‘SelectKBest’ function [54], which was used to select out features in the training set and then applied on the testing set. This function took a numerical value K as an input parameter, applied ANOVA F-test on each feature, and selected out K features with the highest F-score. A linear SVM classifier was trained on the training set with the selected features, and further applied the learned feature weights on the testing set to predict the group label of the testing set. Each LOOCV procedure included S iteration loops. The performance of the LOOCV were evaluated with the classification accuracy calculated on all the testing set.
- S2) In the Q determine process, the input parameter K varied from 1 to J outside the LOOCV procedure, and the LOOCV procedure was performed on each K . The resulted classification accuracies of all LOOCV procedures were compared, and the K value of the best LOOCV performance was assigned to Q .
- S3) After determining the value of Q , another LOOCV procedure was performed using Q as the input parameter for the feature selecting function. The classification performance of LOOCV were summarized in Table III.
- S4) Permutation test was performed by randomly permuting the group labels of the real dataset for 1000 times. With each shuffling, step S3 was performed. The number of times when accuracy and AUC obtained by 1000 permuted dataset were higher than those obtained by real dataset were counted. And the counted number divided by 1000 derived the p-value for the permutation test.

In S3), there was S iteration loops in the whole LOOCV procedure. In each loop, Q features will be selected out from J features in the training set, and the weights of the selected features will be learned by the SVM classifier trained on the training set. It should be noted that the selected Q features may vary slightly across the S iteration loops. We identified

TABLE II
ROIs WITH DIFFERENT LOCAL FCs BETWEEN
FES PATIENTS AND HCs

Metric type	ROIs included regions	Voxel number	Coordinate of peaks (MNI)	t statistic value	ROI value (mean \pm SD)
mean-DRePS	STG_R #	37	(51 -33 3)	5.571	FES: 0.515 \pm 0.054 HCs: 0.477 \pm 0.057
	MTG_R				
	HIP_R #	21	(30 -18 -18)	5.303	FES: 0.435 \pm 0.047 HCs: 0.401 \pm 0.039
	PHG_R				
	PUT_R #, CAU_R	13	(15 15 -6)	4.792	FES: 0.536 \pm 0.066 HCs: 0.491 \pm 0.052
KCC-ReHo	STG_R#	33	(48 -33 6)	5.395	FES: 0.369 \pm 0.069 HCs: 0.323 \pm 0.074
	MTG_R				
	HIP_R #	15	(30 -18 -18)	5.144	FES: 0.266 \pm 0.055 HCs: 0.225 \pm 0.047
	PHG_R				
	PUT_R#, CAU_R	11	(15 15 -6)	4.593	FES: 0.391 \pm 0.086 HCs: 0.334 \pm 0.064
Cohe-ReHo	None #	49	(51 -33 3)	5.482	FES: 0.218 \pm 0.035 HCs: 0.191 \pm 0.025
	CAU_R/L				

Note: Abnormal ROIs where the significant voxel clusters located were denoted by AAL atlas, and the ROIs in which the peak voxel located were marked by #. Temporal_Sup_R (STG), Temporal_Mid_R (MTG), Hippocampus (HIP), ParaHippocampal (PHG), Caudate nucleus (CAU), and Putamen (PUT). left hemisphere (_L), right hemisphere (_R).

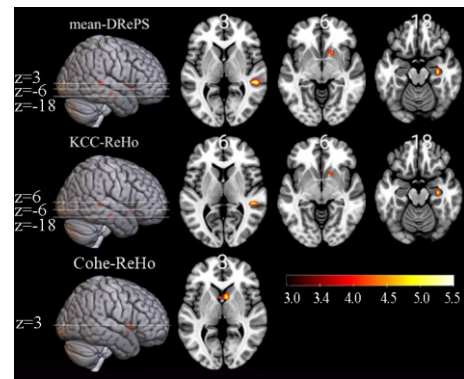


Fig. 2. Group differences of mean-DRePS (first row), KCC-ReHo (second row) and Cohe-ReHo (third row) between FES patients and HCs detected with a two sample t-test statistical analysis. The color bar indicates that FES patients had higher values than HCs. The significance level was FDR-corrected $p < 0.05$, and the size of cluster (i.e., the number of voxels) was greater than 10.

the features that were consistently selected across the S iteration loops as the contributive features, and quantified the contribution of these features with the average the absolute values of the features’ weights across the S iteration loops.

III. RESULTS

A. Group Difference Between FES Patients and HCs

FES patients showed significant increase in mean-DRePS, KCC-ReHo and Cohe-ReHo, mainly in right hemisphere. And no significant reduction of any metric was found. The significant voxel clusters (abnormal ROIs) were shown in Fig. 2 and Table II. Specifically, mean-DRePS exhibited abnormal increase in the right STG, right MTG, right HIP, right PHG, right PUT, and right CAU. KCC-ReHo showed abnormal increase in brain regions similar to mean-DRePS. Cohe-ReHo showed a bilateral increase in CAU in FES patients. No significant difference between FES patients and HCs were found in psd-DRePS, var-DRePS, and zcr-DRePS.

TABLE III

SVM PERFORMANCE FOR CLASSIFYING FES PATIENTS AND HCs

Classification features	Mean accuracy	Permutation p-value	Mean AUC	Permutation p-value	Q	consistent feature number
classifiers applied on single type local FC metrics						
mean-DRePS	0.670	0.051	0.624	0.034	28	19
KCC-ReHo	0.696	0.019	0.644	0.024	31	24
Cohe-ReHo	0.748	0.001	0.739	0.001	66	58
zer-DRePS	0.687	0.032	0.599	0.036	3	1
var-DRePS	0.678	0.040	0.614	0.043	15	11
psd-DRePS	0.635	0.950	0.493	0.951	1	1
classifiers applied on paired local FC metrics						
CoheReHo+KCC-ReHo	0.730	0.004	0.660	0.005	15	7
Cohe-ReHo+mean-DRePS	0.730	<0.001	0.704	<0.001	130	113
Cohe-ReHo+zer-DRePS	0.809	0.002	0.770	0.002	116	95
Cohe-ReHo+var-DRePS	0.722	0.002	0.686	0.003	170	151
Cohe-ReHo+psd-DRePS	0.739	0.003	0.705	0.003	21	10
KCC-ReHo+mean-DRePS	0.704	0.015	0.656	0.014	58	43
KCC-ReHo+zer-DRePS	0.730	0.001	0.704	0.001	120	95
KCC-ReHo+var-DRePS	0.678	0.012	0.641	0.015	88	72
KCC-ReHo+psd-DRePS	0.678	0.036	0.630	0.046	41	25
meanDRePS+zer-DRePS	0.748	0.002	0.739	0.001	111	91
meanDRePS+var-DRePS	0.652	0.049	0.605	0.064	61	50
meanDRePS+psd-DRePS	0.696	0.020	0.655	0.020	43	25
zer-DRePS+var-DRePS	0.713	0.012	0.674	0.009	22	12
zer-DRePS+psd-DRePS	0.687	0.026	0.637	0.031	28	16
var-DRePS+psd-DRePS	0.635	0.903	0.493	0.906	1	1
classifiers applied on static, dynamic and all local FC metrics						
static metrics	0.730	0.003	0.682	0.003	57	39
dynamic metrics	0.713	0.001	0.674	0.003	257	222
all metrics	0.765	0.001	0.731	0.001	66	39

B. Univariate Correlation of Abnormal ROI Values With Respect to Neurocognitive Test Performance and Symptoms

For the seven abnormal ROIs whose static metrics showed significant differences between FES patients and HCs (Table II), we further analyzed univariate correlations of the static metrics of the seven ROIs with respect to the symptoms and cognitive scores respectively. Bonferroni correction was used for multiple comparison correction. According to significant threshold corrected by number of abnormal ROIs ($p < 0.05/7$), a significant correlation was found between the GAF-score of current situation and Cohe-ReHo of ROI in bilateral CAU ($r = -0.336$, $p = 0.004$). As to neurocognitive test performance scores, no correlation passed the Bonferroni correction.

C. Prediction Performance of the RVM Model

According to the results of permutation test, only the GAF-score highest in past year (prediction performance $r = 0.166$, permutation test $p = 0.034$) and the BVMT-R score (prediction performance $r = 0.196$, permutation test

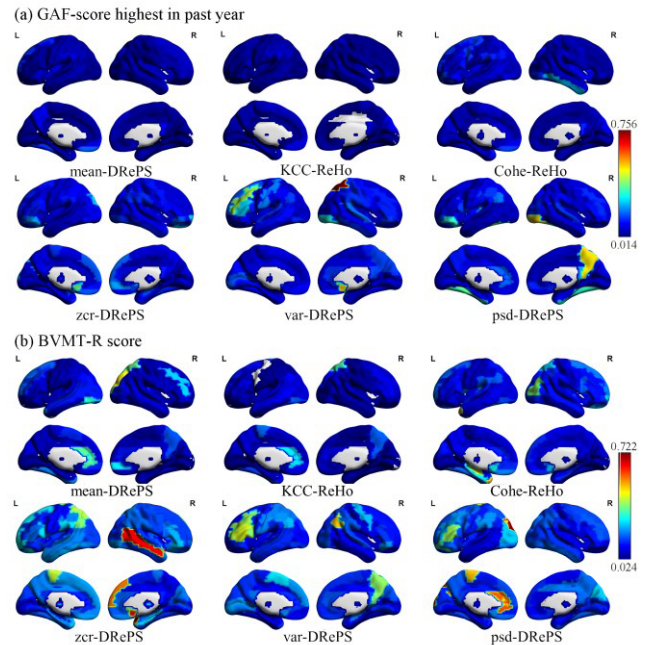


Fig. 3. Surface maps of the contributive ratios of contributive features in the significantly predicted (a) GAF-score highest in past year and (b) BVMT-R score.

$p = 0.014$) were significantly predicted. The contribution of each feature in the two significant predictions was evaluated using the ratio of input features assigned with non-zero weight across the 100 repeated 5-fold training processes. The regional distribution of the contributive ratio of all non-zero weight features in the two significantly predicted scores were arranged by features' metric attribution and shown in Fig. 3. In each successfully predicted models, regional contributive ratio of different metrics showed different spatial patterns. However, the contributive ratio of dynamic metrics were obviously higher than static metrics in many brain regions. The top three contributive features with the highest contributive ratios in the prediction of GAF-score highest in past year were var-DRePS in right superior parietal gyrus (ratio = 0.756), zer-DRePS in right CAU (ratio = 0.542), and var-DRePS in right Olfactory cortex (ratio = 0.538). The top three contributive features with the highest contributive ratios in the prediction of BVMT-R score were psd-DRePS in left superior occipital gyrus (ratio = 0.722), zer-DRePS in right temporal pole (Temporal_Pole_Sup_R, ratio = 0.706), and the zer-DRePS in right MTG (ratio = 0.642). The contributive ratios of all contributive features and full region names of AAL atlas were organized in the Supplementary Tables S1 and S2.

D. Classification Performance of the SVM Model

We evaluated the diagnostic ability of the input features formed by single type local FC metric, any paired local FC metrics, combinations of all static local FC metrics, combinations of all dynamic local FC metrics, and combinations of all local FC metrics (Table III). Linear SVM classifiers were applied on these input features. The performances of classifiers were evaluated by classification accuracy and AUC

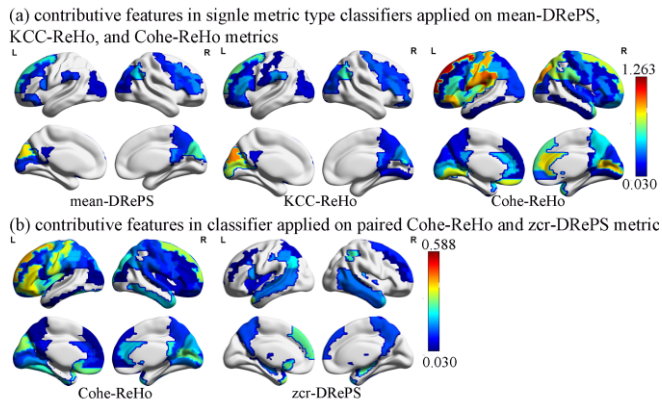


Fig. 4. (a) The contribution of identified contributive features in classifiers applied on single type metrics, including Cohe-ReHo, KCC-ReHo and mean-DRePS. (b) The contribution of identified contributive features in the classifier showed the highest classification accuracy, which was applied on input feature space formed with paired Cohe-ReHo and zcr-DRePS metrics. The contribution was calculated by averaging the absolute weights learned by linear SVM classifier across S iteration loops in LOOCV.

calculated with the LOOCV. In each iteration loop of LOOCV, 125 samples were randomly split into 124 training sample and 1 testing sample, a feature selection option was used to select out Q highest F-value scored features from the input features in training set, linear SVM classifier was trained on training set by the selected Q features, and the learned feature weights were further applied on the testing sample to estimate its group label. We gradually increased Q from 1 to J , and recorded the accuracy obtained with LOOCV under each Q . The final value of Q for each feature space was recorded based on the highest classification accuracy achieved by the classifier. As the selected Q features may vary across the LOOCV loops, we recorded the features that were consistently selected across the loops as contributive features, and presented their number in Table III. The contribution of identified contributive features was quantified with the average of absolute feature weights across S LOOCV loops. The best classification performance was achieved by the linear SVM classifier trained with features formed by pairing the Cohe-ReHo metric with the zcr-DRePS metric. This configuration yielded an accuracy of 80.9% (permutation test $p = 0.002$), an AUC of 77.0% (permutation test $p = 0.001$), a sensitivity of 90.5% (permutation test $p < 0.001$), and a specificity of 81.7% (permutation test $p < 0.001$) when 116 features were selected.

We examined the contribution of contributive features in classifiers applied on single type local FC metrics and the classifier obtained best classification performance (Fig. 4a-b).

In classifiers applied on single type local FC metrics, we concentrated on contributive features overlapped with the ROIs that showed group difference (Table II) in brain regions defined by AAL atlas (Fig. 4a). For the Cohe-ReHo metric, such overlapping appeared in feature in right CAU (average weight = 1.264, rank = 1) and feature in right STG (average weight = 0.231, rank = 40). And there was no such overlapping in classifiers applied on mean-DRePS and KCC-ReHo metrics. In classifier applied on paired Cohe-ReHo and

zcr-DRePS metrics, the top three contributive features were the feature in right CAU derived from Cohe-ReHo metric (average weight = 0.569, rank = 1), the feature in right PUT derived from zcr-DRePS metric (average weight = 0.512, rank = 2), and the feature in left Superior frontal gyrus derived from Cohe-ReHo metric (average weight = 0.408, rank = 3).

We examined the influence of dynamic metrics on the classification performance. The performances of the classifiers applied on single type dynamic metrics were inferior to the classifiers applied on single type static metrics (Table III). The accuracy and AUC of classifiers applied on all metrics were higher than classifiers applied on static metrics. However, not all dynamic metrics were useful for improving classification performance when combined with static metrics. In particular, only the zcr-DRePS metric could improve the performance of classifiers when it was paired with single static metrics.

IV. DISCUSSION

In this study, one newly developed dynamic local FC analysis method (i.e., DRePS) and two commonly used static local FC analysis methods (i.e., KCC-ReHo and Cohe-ReHo) were used to investigate the alterations of local brain spontaneous activities in FES patients. Prediction and classification analysis were conducted to examine and compare the clinical application potential of the dynamic and static local FC metrics derived from DRePS, KCC-ReHo and Cohe-ReHo methods. Results showed that FES patients exhibited increased static local FC in some brain regions, which had correlations with GAF score of current situation in patients, and the dynamic local FC metric zcr-DRePS combined with static local FC metrics may have better performance than the cases when only static local FC metrics were used as features in classification.

A. Static Local FC Metrics Indicate Group-Level Alterations in FES Patients

Regional alterations in FES patients were found in right STG, right MTG, right HIP, right PHG, right PUT, and bilateral CAU in terms of the static local FC metrics, i.e., mean-DRePS, KCC-ReHo and Cohe-ReHo. The detected ROIs with abnormal local static FC are partly consistent with previous studies. In detail, altered ReHo or ALFF in PUT, STG and MTG regions in FES patients or chronic schizophrenia patients has been reported. For example, a meta-analysis study found altered ReHo in PUT in drug-naïve FES patients [13]. Increased ReHo in the bilateral PUTs was also observed in FES patients compared to HCs [55]. Altered ReHo values in temporal cortex in FES patients [56], [57], and increased ReHo in bilateral striatum, and medial temporal cortex in chronic schizophrenia patients [58] have been reported. Correlation between mean-DRePS and KCC-ReHo has been observed in previous studies [28], [40], and correlation between Cohe-ReHo and KCC-ReHo was reported as well [45]. These results may explain why the three local FC analysis methods indicated a similar spatial distribution of altered static local FC in FES patients (Fig. 2 and TABLE II). However, alterations in CAU and HIP were seldom reported in previous schizophrenia research. CAU and

HIP have important role in schizophrenia. The CAU is a part of dorsal striatum, and the HIP affects the dopamine pathway. Both of them are related to the dysfunction of the dopaminergic system in schizophrenia [59], [60].

However, no significant regional alteration was detected in terms of the dynamic local FC metrics (i.e., zcr-DRePS, var-DRePS and psd-DRePS). This suggests that dynamic metrics capture different aspects of local FC compared to static metrics. It is worth noting that dynamic metrics have successfully detected group differences in studies of generalized anxiety disorder [39] and neocortical focal epilepsy [40]. Therefore, there is potential for developing new dynamic metrics based on DRePS, which warrants further exploration in schizophrenia research.

B. Dynamic Local FC Metrics Correlate With Clinical Characteristics

By using the RVM model, we found that the GAF-score highest in the past year and the BVMT-R score could be significantly predicted by input features formed with both static and dynamic local FC metrics. Additionally, in the two successfully prediction models, most of the contributive features with high contribution ratio belonged to dynamic local FC metrics (Supplementary Tables S1 and S2, and Fig. 3). However, neither the two scores showed significant correlation with the abnormal ROIs that had significant difference between FES patients and HCs (Table II). These findings suggest that the association between the two clinical scores and local FC metrics revealed by RVM prediction model can supplement the association observed through the lens of univariate correlation statistical analysis. Achieving reproducible or robust relationships between brain neuroimaging and clinical phenotypes remains a bottleneck problem for building better biomarkers [3], [5], [7], [8]. Using machine learning analysis and dynamic FC analysis may contribute to relevant research [8], [23], [24], [42], [61], [62], [63]. A previous study revealed an association between node average controllability and the general and positive dimension from PANSS scores [64]. Since controllability metrics incorporate network-level FC information, we speculate that neuroimaging biomarkers associated with symptoms should perhaps be developed by combining the information of both static FC and dynamic FC at both the network-level scale and the local spatial scale.

C. Dynamic Local FC Metrics Improves the Performance of Classification

In this study, we performed the classification analysis from [22], which used dynamic state characteristics and regional dynamic topology properties as input features for linear SVM classifier. The highest accuracy in our study (accuracy = 80.9% permutation test $p = 0.002$) was slightly higher than the results reported in reference (accuracy = 72.3%, permutation test $p < 0.001$) [22]. Previous studies that applied SVM on input features formed with local FC metrics reported classification accuracy ranging from 78.5% to 98.1% [65], [66], [67], [68], [69]. The difference of classification accuracies among these studies and our study may due to

the factors including sample size, feature selection processes, kernel function, and validation processes. It is difficult to conclude which classification analysis performed better simply by comparing accuracies across different studies.

By comparing the accuracies of all classifiers in this study, we found that although the diagnostic value of dynamic metrics is not higher than static metrics when used separately, better classification performance could be achieved when combining them. The contribution of zcr-DRePS in improving classification accuracy was prominent (Table III). This view can be concluded by comparing the performance of classifiers applied on single type local FC metrics and classifiers applied on local FC metrics paired with zcr-DRePS. Previous study applied linear SVM on static and dynamic network level FC (FNC) features, and found that the classification using both dynamic and static FNC features significantly outperformed the classification using only static FNC features [70]. Our study provides additional evidence for the value of incorporating dynamic local FC metrics with static local FC metrics in the development of a diagnostic biomarker for psychosis.

D. The Importance of CAU and Zcr-DRePS in Machine Learning Analysis

The brain regions involved in contributive features identified in prediction analysis and classification analysis were not all consistent with abnormal ROIs that had significant difference between groups. In prediction model of GAF-score highest in past year, the top 15% contributive features involved the zcr-DRePS, KCC-ReHo and Cohe-ReHo of CAU_R (Supplementary Table S1). In prediction model of BVMT-R score, the zcr-DRePS of MTG_R, STG_R and CAU_R were among the top 10 contributive features (Supplementary Table S2). In all classifiers applied on input features involved Cohe-ReHo and/or zcr-DRePS metrics, especially classifier applied on paired Cohe-ReHo and zcr-DRePS metrics, the contribution of the identified contributive features in these classifier emphasized the importance of the features of Cohe-ReHo in CAU_R and the features of zcr-DRePS in PUT_R, CAU_R and STG_R in classification FES patients and HCs (Supplementary Tables S3 and S4 and Fig. 4). These results together suggested that among all the abnormal ROIs, the CAU was the most contributive region in prediction analysis and classification analysis. And among all the metrics, Cohe-ReHo and zcr-DRePS are most valuable for developing prognosis and diagnosis biomarker in schizophrenia.

E. Limitations

Several limitations should be considered in this study. First, our findings were not validated in an independent dataset. Though we carefully designed the repetition of cross validation and permutation test (1000 times), the results need further independent study to ensure the reliability. Second, the scan length of the rs-fMRI data used in this study is relatively short (5.83 min). Generally, a longer duration of fMRI data is required in the dynamic FC analysis, especially for the dynamic FC analysis based on sliding windows. The typical acquisition scan length of rs-fMRI in humans is 5-10 min [19].

Previous studies have shown that the reliability of static FC metrics changes in a saturating exponential manner with the increase of scan length [71], [72], and scan length required to achieve stable static FC varied across different metrics [73]. In this study, we examined the dynamic local FC based on DRePS, which could quantify the instantaneous phase synchronization in local region with high temporal resolution. We note that though DRePS is with high temporal resolution, it also has limitation, that is, it does not take the instantaneous amplitude of fMRI time series into consideration and thus cannot reflect the relationship of the amplitude information of fMRI time series in local region. Anyway, further studies with longer fMRI scan length are needed to examine the effect of scan length on DRePS analysis. Third, the FES patients in our study were drug-naïve and free from any psychiatric comorbidities. While studying the first-episode phase is important for directly investigating the mechanisms of schizophrenia, it may limit the generalizability of our findings to patients with comorbidities. Further studies are needed to verify these results.

V. CONCLUSION

To conclude, this study comprehensively investigated the alterations of local FC in FES patients using three local FC analysis methods, i.e., DRePS, KCC-ReHo, and Cohe-ReHo. Results showed that static local FC metrics were more sensitive than dynamic local FC metrics in detecting alterations of brain activity in FES patients, while dynamic local FC metrics, combined with static local FC metrics, could also contribute to improve prediction of FES symptoms and classification of FES patients from HCs. RVM prediction model revealed associations between all dynamic metrics and GAF-score highest in past year and BVMT-R score, which may have been overlooked in univariate correlation analysis. The highly contribution of dynamic local FC metrics in prediction analysis indicated the importance of dynamic FC in constructing robust association between brain neuroimaging and clinical phenotypes. Linear SVM based classification with a combination of static and dynamic local FC features, particularly incorporating zcr-DRePS as a dynamic metric, achieved better classification performance than using static local FC metrics alone. The contributive features in classification analysis involved more with CAU region and zcr-DRePS and Cohe-ReHo metrics. These findings highlight the potential of developing dynamic metrics from DRePS and applying them in the development of diagnostic biomarkers.

REFERENCES

- [1] R. A. McCutcheon, T. Reis Marques, and O. D. Howes, "Schizophrenia—An overview," *JAMA Psychiatry*, vol. 77, no. 2, pp. 201–210, Feb. 2020.
- [2] E. Walker, L. Kestler, A. Bollini, and K. M. Hochman, "Schizophrenia: Etiology and course," *Annu. Rev. Psychol.*, vol. 55, no. 1, pp. 401–430, Feb. 2004.
- [3] N. V. Kraguljac, W. M. McDonald, A. S. Widge, C. I. Rodriguez, M. Tohen, and C. B. Nemeroff, "Neuroimaging biomarkers in schizophrenia," *Amer. J. Psychiatry*, vol. 178, no. 6, pp. 509–521, Jun. 2021.
- [4] M. Kubicki and M. E. Shenton, Eds., *Neuroimaging Schizophrenia*. Cham, Switzerland: Springer, 2020.
- [5] C.-W. Woo, L. J. Chang, M. A. Lindquist, and T. D. Wager, "Building better biomarkers: Brain models in translational neuroimaging," *Nature Neurosci.*, vol. 20, no. 3, pp. 365–377, Feb. 2017.
- [6] G. Orru, W. Pettersson-Yeo, A. F. Marquand, G. Sartori, and A. Mechelli, "Using support vector machine to identify imaging biomarkers of neurological and psychiatric disease: A critical review," *Neurosci. Biobehavioral Rev.*, vol. 36, no. 4, pp. 1140–1152, Apr. 2012.
- [7] S. Marek et al., "Reproducible brain-wide association studies require thousands of individuals," *Nature*, vol. 603, no. 7902, pp. 654–660, Mar. 2022.
- [8] M. D. Rosenberg and E. S. Finn, "How to establish robust brain-behavior relationships without thousands of individuals," *Nature Neurosci.*, vol. 25, no. 7, pp. 835–837, Jul. 2022.
- [9] J. Li, Y. Sun, Y. Huang, A. Bezerianos, and R. Yu, "Machine learning technique reveals intrinsic characteristics of schizophrenia: An alternative method," *Brain Imag. Behav.*, vol. 13, no. 5, pp. 1386–1396, Oct. 2019.
- [10] J. Chen et al., "Intrinsic connectivity patterns of task-defined brain networks allow individual prediction of cognitive symptom dimension of schizophrenia and are linked to molecular architecture," *Biol. Psychiatry*, vol. 89, no. 3, pp. 308–319, Feb. 2021.
- [11] B. Biswal, F. Z. Yetkin, V. M. Haughton, and J. S. Hyde, "Functional connectivity in the motor cortex of resting human brain using echo-planar MRI," *Magn. Reson. Med.*, vol. 34, no. 4, pp. 537–541, 1995.
- [12] L. Jiang and X.-N. Zuo, "Regional homogeneity: A multimodal, multi-scale neuroimaging marker of the human connectome," *Neuroscientist*, vol. 22, no. 5, pp. 486–505, Oct. 2016.
- [13] X. Qiu et al., "Alterations in spontaneous brain activity in drug-naïve first-episode schizophrenia: An anatomical/activation likelihood estimation meta-analysis," *Psychiatry Invest.*, vol. 19, no. 8, pp. 606–613, Aug. 2022.
- [14] X. Shan et al., "Increased regional homogeneity modulated by metacognitive training predicts therapeutic efficacy in patients with schizophrenia," *Eur. Arch. Psychiatry Clin. Neurosci.*, vol. 271, no. 4, pp. 783–798, Jun. 2021.
- [15] X. Qiu et al., "Regional homogeneity brain alterations in schizophrenia: An activation likelihood estimation meta-analysis," *Psychiatry Invest.*, vol. 18, no. 8, pp. 709–717, Aug. 2021.
- [16] R. Yu et al., "Frequency-specific alternations in the amplitude of low-frequency fluctuations in schizophrenia," *Hum. Brain Mapping*, vol. 35, no. 2, pp. 627–637, Feb. 2014.
- [17] Z. Fu et al., "Characterizing dynamic amplitude of low-frequency fluctuation and its relationship with dynamic functional connectivity: An application to schizophrenia," *NeuroImage*, vol. 180, pp. 619–631, Oct. 2018.
- [18] J. A. Hadley, N. V. Kraguljac, D. M. White, L. Ver Hoef, J. Tabora, and A. C. Lahti, "Change in brain network topology as a function of treatment response in schizophrenia: A longitudinal resting-state fMRI study using graph theory," *NPJ Schizophrenia*, vol. 2, no. 1, pp. 1–7, Apr. 2016.
- [19] R. M. Hutchison et al., "Dynamic functional connectivity: Promise, issues, and interpretations," *NeuroImage*, vol. 80, pp. 360–378, Oct. 2013.
- [20] D. J. Lurie et al., "Questions and controversies in the study of time-varying functional connectivity in resting fMRI," *Netw. Neurosci.*, vol. 4, no. 1, pp. 30–69, Jan. 2020.
- [21] M. G. Preti, T. A. Bolton, and D. Van De Ville, "The dynamic functional connectome: State-of-the-art and perspectives," *NeuroImage*, vol. 160, pp. 41–54, Oct. 2017.
- [22] W. You et al., "Impaired dynamic functional brain properties and their relationship to symptoms in never treated first-episode patients with schizophrenia," *Schizophrenia*, vol. 8, no. 1, p. 90, Oct. 2022.
- [23] L. Luo, W. You, M. P. DelBello, Q. Gong, and F. Li, "Recent advances in psychoradiology," *Phys. Med. Biol.*, vol. 67, no. 23, Dec. 2022, Art. no. 23TR01.
- [24] L. Luo et al., "Shared and disorder-specific alterations of brain temporal dynamics in obsessive-compulsive disorder and schizophrenia," *Schizophrenia Bull.*, vol. 49, no. 5, pp. 1387–1398, Sep. 2023.
- [25] E. D. Meram et al., "The topology, stability, and instability of learning-induced brain network repertoires in schizophrenia," *Netw. Neurosci.*, vol. 7, no. 1, pp. 184–212, Jan. 2023.
- [26] M. Pedersen, A. Omidvarnia, J. M. Walz, A. Zalesky, and G. D. Jackson, "Spontaneous brain network activity: Analysis of its temporal complexity," *Netw. Neurosci.*, vol. 1, no. 2, pp. 100–115, Jun. 2017.

- [27] L. Deng, J. Sun, L. Cheng, and S. Tong, "Characterizing dynamic local functional connectivity in the human brain," *Sci. Rep.*, vol. 6, no. 1, May 2016, Art. no. 26976.
- [28] J. Zhou, H. Zhu, J. Wang, and J. Sun, "Dynamic characteristics of local functional connectivity revealed by dynamic regional phase synchrony," *IEEE Trans. Neural Syst. Rehabil. Eng.*, vol. 31, pp. 2507–2517, 2023.
- [29] Z. Liao et al., "Altered dynamic intrinsic brain activity of the default mode network in Alzheimer's disease: A resting-state fMRI study," *Frontiers Hum. Neurosci.*, vol. 16, Aug. 2022, Art. no. 951114.
- [30] K. Xue et al., "Local dynamic spontaneous brain activity changes in first-episode, treatment-naïve patients with major depressive disorder and their associated gene expression profiles," *Psychol. Med.*, vol. 52, no. 11, pp. 2052–2061, Aug. 2022.
- [31] J. Chen et al., "Dynamic alterations in spontaneous neural activity in multiple brain networks in subacute stroke patients: A resting-state fMRI study," *Frontiers Neurosci.*, vol. 12, p. 994, Jan. 2019.
- [32] Y. Zhang, G. Guo, and Y. Tian, "Increased temporal dynamics of intrinsic brain activity in sensory and perceptual network of schizophrenia," *Frontiers Psychiatry*, vol. 10, p. 484, Jul. 2019.
- [33] J. Zhu, D.-M. Zhu, Y. Qian, X. Li, and Y. Yu, "Altered spatial and temporal concordance among intrinsic brain activity measures in schizophrenia," *J. Psychiatric Res.*, vol. 106, pp. 91–98, Nov. 2018.
- [34] B. Bohaterewicz et al., "Machine learning-based identification of suicidal risk in patients with schizophrenia using multi-level resting-state fMRI features," *Frontiers Neurosci.*, vol. 14, Jan. 2021, Art. no. 605697.
- [35] P. J. Uhlhaas and W. Singer, "Oscillations and neuronal dynamics in schizophrenia: The search for basic symptoms and translational opportunities," *Biol. Psychiatry*, vol. 77, no. 12, pp. 1001–1009, Jun. 2015.
- [36] J. R. da Cruz et al., "EEG microstates are a candidate endophenotype for schizophrenia," *Nature Commun.*, vol. 11, no. 1, p. 3089, Jun. 2020.
- [37] J. Sun et al., "Abnormal time dynamics of EEG oscillations in schizophrenia patients on multiple time scales," *IEEE Trans. Biomed. Eng.*, vol. 61, no. 6, pp. 1756–1764, Jun. 2014.
- [38] A. Omidvarnia, M. Pedersen, J. M. Walz, D. N. Vaughan, D. F. Abbott, and G. D. Jackson, "Dynamic regional phase synchrony (DRePS): An instantaneous measure of local fMRI connectivity within spatially clustered brain areas," *Hum. Brain Mapping*, vol. 37, no. 5, pp. 1970–1985, May 2016.
- [39] Q. Cui et al., "Disrupted dynamic local brain functional connectivity patterns in generalized anxiety disorder," *Prog. Neuro-Psychopharmacol. Biol. Psychiatry*, vol. 99, Apr. 2020, Art. no. 109833.
- [40] M. Pedersen, A. Omidvarnia, E. K. Curwood, J. M. Walz, G. Rayner, and G. D. Jackson, "The dynamics of functional connectivity in neocortical focal epilepsy," *NeuroImage, Clin.*, vol. 15, pp. 209–214, Jan. 2017.
- [41] Q. Tang et al., "Shared and distinct changes in local dynamic functional connectivity patterns in major depressive and bipolar depressive disorders," *J. Affect. Disorders*, vol. 298, pp. 43–50, Feb. 2022.
- [42] X. Wu et al., "Dynamic changes in brain lateralization correlate with human cognitive performance," *PLOS Biol.*, vol. 20, no. 3, Mar. 2022, Art. no. e3001560.
- [43] K. Maurice and G. Jean Dickinson, *Rank Correlation Methods*, 5th ed. London, U.K.: Oxford Univ. Press, 1990.
- [44] Y. Zang, T. Jiang, Y. Lu, Y. He, and L. Tian, "Regional homogeneity approach to fMRI data analysis," *NeuroImage*, vol. 22, no. 1, pp. 394–400, May 2004.
- [45] D. Liu, "Using coherence to measure regional homogeneity of resting-state fMRI signal," *Frontiers Syst. Neurosci.*, vol. 4, p. 1366, Jun. 2010.
- [46] American Psychiatric Association, DSM-5, and American Psychiatric Association, Eds., *Diagnostic and Statistical Manual of Mental Disorders: DSM-5*, vol. 5, 5th ed. Washington, DC, USA: American Psychiatric Association, 2013.
- [47] C.-G. Yan, X.-D. Wang, X.-N. Zuo, and Y.-F. Zang, "DPABI: Data processing & analysis for (resting-state) brain imaging," *Neuroinformatics*, vol. 14, no. 3, pp. 339–351, Jul. 2016.
- [48] J. Ashburner et al., *SPM12 Manual*, vol. 2464, no. 4. London, U.K.: Wellcome Trust Centre for Neuroimaging, 2014.
- [49] X.-Z. Jia et al., "RESTplus: An improved toolkit for resting-state functional magnetic resonance imaging data processing," *Sci. Bull.*, vol. 64, no. 14, pp. 953–954, Jul. 2019.
- [50] J. Sun and M. Small, "Unified framework for detecting phase synchronization in coupled time series," *Phys. Rev. E, Stat. Phys. Plasmas Fluids Relat. Interdiscip. Top.*, vol. 80, no. 4, Oct. 2009, Art. no. 046219.
- [51] X.-N. Zuo et al., "The oscillating brain: Complex and reliable," *NeuroImage*, vol. 49, no. 2, pp. 1432–1445, Jan. 2010.
- [52] N. Tzourio-Mazoyer et al., "Automated anatomical labeling of activations in SPM using a macroscopic anatomical parcellation of the MNI MRI single-subject brain," *NeuroImage*, vol. 15, no. 1, pp. 273–289, Jan. 2002.
- [53] M. E. Tipping, "Sparse Bayesian learning and the relevance vector machine," *J. Mach. Learn. Res.*, vol. 1, pp. 211–244, Jun. 2001.
- [54] F. Pedregosa et al., "Scikit-learn: Machine Learning in Python," *J. Mach. Learn. Res.*, vol. 12, pp. 2825–2830, Nov. 2011.
- [55] L.-B. Cui et al., "Putamen-related regional and network functional deficits in first-episode schizophrenia with auditory verbal hallucinations," *Schizophrenia Res.*, vol. 173, nos. 1–2, pp. 13–22, May 2016.
- [56] X. Zhao et al., "Abnormalities of regional homogeneity and its correlation with clinical symptoms in Naïve patients with first-episode schizophrenia," *Brain Imag. Behav.*, vol. 13, no. 2, pp. 503–513, Apr. 2019.
- [57] H. Lyu et al., "Abnormal causal connectivity of left superior temporal gyrus in drug-naïve first-episode adolescent-onset schizophrenia: A resting-state fMRI study," *Psychiatry Res., Neuroimaging*, vol. 315, Sep. 2021, Art. no. 111330.
- [58] Y. Xu, C. Zhuo, W. Qin, J. Zhu, and C. Yu, "Altered spontaneous brain activity in schizophrenia: A meta-analysis and a large-sample study," *BioMed Res. Int.*, vol. 2015, pp. 1–11, Oct. 2015.
- [59] J. Epstein, E. Stern, and D. Silbersweig, "Mesolimbic activity associated with psychosis in schizophrenia: Symptom-specific PET studies," *Ann. New York Acad. Sci.*, vol. 877, no. 1, pp. 562–574, Jun. 1999.
- [60] D. Lodge and S. Perez, "New approaches to the management of schizophrenia: Focus on aberrant hippocampal drive of dopamine pathways," *Drug Design, Develop. Therapy*, vol. 8, p. 887, Jul. 2014.
- [61] L. Luo et al., "Patterns of brain dynamic functional connectivity are linked with attention-deficit/hyperactivity disorder-related behavioral and cognitive dimensions," *Psychol. Med.*, vol. 53, no. 14, pp. 6666–6677, Feb. 2023.
- [62] E. S. Finn and P. A. Bandettini, "Movie-watching outperforms rest for functional connectivity-based prediction of behavior," *NeuroImage*, vol. 235, Jul. 2021, Art. no. 117963.
- [63] J. Li et al., "Global signal regression strengthens association between resting-state functional connectivity and behavior," *NeuroImage*, vol. 196, pp. 126–141, Aug. 2019.
- [64] Q. Li et al., "Controllability of functional brain networks and its clinical significance in first-episode schizophrenia," *Schizophrenia Bull.*, vol. 49, no. 3, pp. 659–668, May 2023.
- [65] Y. Liu, Y. Zhang, L. Lv, R. Wu, J. Zhao, and W. Guo, "Abnormal neural activity as a potential biomarker for drug-naïve first-episode adolescent-onset schizophrenia with coherence regional homogeneity and support vector machine analyses," *Schizophrenia Res.*, vol. 192, pp. 408–415, Feb. 2018.
- [66] S. Wang et al., "Abnormal regional homogeneity as a potential imaging biomarker for adolescent-onset schizophrenia: A resting-state fMRI study and support vector machine analysis," *Schizophrenia Res.*, vol. 192, pp. 179–184, Feb. 2018.
- [67] S. Gao et al., "Association of reduced local activities in the default mode and sensorimotor networks with clinical characteristics in first-diagnosed episode of schizophrenia," *Neuroscience*, vol. 495, pp. 47–57, Jul. 2022.
- [68] S. Gao et al., "Enhanced prefrontal regional homogeneity and its correlations with cognitive dysfunction/psychopathology in patients with first-diagnosed and drug-naïve schizophrenia," *Frontiers Psychiatry*, vol. 11, Oct. 2020, Art. no. 580570.
- [69] F. Wu et al., "Structural and functional brain abnormalities in drug-naïve, first-episode, and chronic patients with schizophrenia: A multimodal MRI study," *Neuropsychiatric Disease Treatment*, vol. 14, pp. 2889–2904, Oct. 2018.
- [70] B. Rashid et al., "Classification of schizophrenia and bipolar patients using static and dynamic resting-state fMRI brain connectivity," *NeuroImage*, vol. 134, pp. 645–657, Jul. 2016.
- [71] R. M. Birn et al., "The effect of scan length on the reliability of resting-state fMRI connectivity estimates," *NeuroImage*, vol. 83, pp. 550–558, Dec. 2013.
- [72] J. Gonzalez-Castillo et al., "The spatial structure of resting state connectivity stability on the scale of minutes," *Frontiers Neurosci.*, vol. 8, p. 138, Jun. 2014.
- [73] D. G. Tomasi, E. Shokri-Kojori, and N. D. Volkow, "Temporal evolution of brain functional connectivity metrics: Could 7 min of rest be enough?" *Cerebral Cortex*, vol. 27, no. 8, pp. 4153–4165, Aug. 2017.